scientific reports

Check for updates

OPEN

Transcriptome analysis combined with single-cell analysis identified that APOC1 influences cholesterol transport by macrophages in ccRCC

Fengran Guo[1,3], Ziyang Ma[1], Hu Wang[2] & Zhenwei Han[1✉]

Renal cell carcinoma (RCC) is one of the most prevalent categories of cancer worldwide, accounting for approximately 2% of cancer diagnoses and cancer deaths worldwide. various immunotherapeutic strategies have emerged as key approaches to managing advanced RCC. Bioinformatics methodologies were employed to analyze the TCGA-KIRC RNA sequencing dataset, GSE105261, GSE168845, and single-cell dataset GSE121636. Various techniques, including PCR, Western blotting, migration assays, scratch wound assays, flow cytometry, and immunofluorescence staining, were utilized to elucidate the functional characteristics of the tumor. In this study, we obtained transcriptome RNA sequencing data from the Cancer Genome Atlas (TCGA) database. Using the ESTIMATE algorithm, 249 immune-related genes were identified. Additionally, single-cell RNA sequencing data were integrated to determine the immune-related genes that affect the prognosis of clear cell renal cell carcinoma (ccRCC). Eventually, a total of 42 immune-related genes (IMDGs) were identified. Subsequently, in vitro experiments confirmed that APOC1 is highly expressed in ccRCC and significantly affects the migration and proliferation of ccRCC cells. Furthermore, our findings indicate that APOC1 plays a critical role in modulating cholesterol transport within macrophages and significantly contributes to the polarization of macrophages toward the M2 phenotype.

Renal cell carcinoma (RCC) is one of the most prevalent categories of cancer worldwide, accounting for approximately 2% of cancer diagnoses and cancer deaths worldwide[1]. Renal cell carcinoma (RCC) is a malignancy that arises from the renal tubular epithelium, constituting more than 90% of all kidney cancer cases[2,3]. Among them, clear cell renal cell carcinoma (ccRCC) is the most common and the cause of most kidney cancer-related deaths[4]. Currently, the primary treatment for localized ccRCC remains surgical resection or ablation[5]. However, patients with advanced disease often experience suboptimal treatment outcomes. Particularly in individuals with metastatic kidney cancer, there is an elevated risk of local or distant metastasis, which further exacerbates the prognosis for these patients[6]. This underscores the critical need for research into immunotherapy and targeted therapies[7]. In recent years, various immunotherapeutic strategies—including monotherapies and combination therapies utilizing anti-PD-1, anti-PD-L1, and anti-CTLA-4 antibodies—as well as tyrosine kinase inhibitor (TKI) targeted therapy have emerged as key approaches to managing advanced RCC[8]. Nevertheless, immunotherapy demonstrates efficacy in only a subset of solid tumors and certain hematologic malignancies. A significant proportion of patients undergoing immunotherapy develop primary and/or acquired resistance, ultimately resulting in treatment failure[9]. Therefore, it is imperative to identify novel therapeutic targets to enhance clinical outcomes in ccRCC.

In recent years, the tumor microenvironment (TME) has emerged as a critical determinant of tumor progression and therapeutic response, making it a focal point in cancer research[10]. The TME consists of diverse cellular elements and molecular factors, including tumor-associated immune cells, fibroblasts, endothelial cells, extracellular matrix components, growth factors, hormones, and cytokines[11]. Among these constituents, tumor-associated macrophages (TAMs) have garnered significant attention due to their pivotal role in tumor development.

[1]Department of Urology, Second Hospital of Hebei Medical University, 215 West Heping Road, Shijiazhuang 050000, China. [2]Department of Urology, First Hospital of Jiaxing, Jiaxing 314033, China. [3] West China Hospital of Sichuan University, Department of Urology, Chengdu, China. ✉email: hanzhenwei@hebmu.edu.cn

TAMs constitute a major immune cell population within the TME, representing approximately 50% of infiltrating cells[12]. These cells can polarize into two distinct phenotypes: M1 and M2. M1 macrophages exhibit anti-tumor properties by producing pro-inflammatory cytokines such as interleukin-6 (IL-6), IL-12, and interferon-γ (IFN-γ), which stimulate robust immune responses[13]. Conversely, M2 macrophages possess pro-tumor characteristics, secreting anti-inflammatory and immunosuppressive factors like IL-13 and transforming growth factor-β (TGF-β)[14]. These factors are closely associated with tumor growth, angiogenesis, metastasis, and adverse clinical outcomes.

The metabolic symbiosis between TAMs and tumor cells is a fundamental aspect of the cancer ecosystem. This interaction not only facilitates tumor cell survival and proliferation but also creates unique adaptive conditions within the TME[15]. Consequently, investigating the metabolic coupling mechanisms between TAMs and tumor cells may provide novel insights for ccRCC treatment strategies. Targeting TAMs and reprogramming their functional states to enhance anti-tumor immunity has become an emerging focus in cancer research.

Apolipoprotein C1 (APOC1) is a member of the apolipoprotein family and plays a crucial role in the metabolism of very-low-density lipoprotein (VLDL) and high-density lipoprotein (HDL)[16]. APOC1 has been implicated in the progression of various diseases, including glomerulosclerosis, diabetes, polycystic ovary syndrome, and Alzheimer's disease[17]. Recent studies have increasingly highlighted the significant role of APOC1 in tumor progression, particularly in cancers such as lung, prostate, and ccRCC[18–20]. Advances in single-cell sequencing technology have provided deeper insights into the interactions between different cellular components within TME and tumor cells. Investigating the function of APOC1 in macrophages within the TME and its influence on ccRCC metastasis may offer novel immunotherapeutic strategies for preventing cancer development and metastasis.

In this study, we conducted research on novel targeted immunotherapy candidate drugs based on the multi- and transcriptomic data as well as single-cell data of renal clear cell carcinoma. We obtained transcriptome RNA sequencing data from The Cancer Genome Atlas (TCGA) database. The ESTIMATE algorithm was employed to quantify the proportions of immune and stromal components in ccRCC samples. A comparative analysis between high-immune and low-immune groups revealed that immune components are more predictive of overall survival (OS) in ccRCC patients. Through differential expression analysis based on these immune group classifications, we identified 249 immune-related genes. Additionally, single-cell RNA sequencing data were integrated to identify immune-related genes influencing ccRCC prognosis. Ultimately, a total of 42 immune-related genes (IMDGs) were identified. By intersecting these IMDGs with differentially expressed genes in the ccRCC dataset, immunohistochemistry confirmed that APOC1 is highly expressed in renal clear cell carcinoma. In vitro experiments demonstrated that APOC1 affects the migration and proliferation of ccRCC cells and plays a significant role in the polarization of macrophages toward the M2 phenotype. Our findings suggest that APOC1 may serve as a potential immunological predictive biomarker, elucidating possible mechanisms underlying tumor initiation and progression.

Method
Datasets
Download TCGA-KIRC RNA seq-data (538 primary tumor and 72 normal tissue samples) and corresponding clinical information from UCSC Xena (xenabrowser.net). Transcriptome data GSE105261, GSE168845, and single-cell dataset GSE121636(3 tumor and 3 normal data) were downloaded from GEO database (Home—GEO—NCBI (nih.gov)). The dataset was selected from the data related to kidney cancer on the GEO website. We did not conduct any special screening on it.

Patients
This study has been approved by the ethics committee. All patient specimens were obtained from the Second Hospital of Hebei Medical University. The study was conducted in accordance with the principles of the Helsinki Declaration. Before the surgery, written informed consent was obtained from all patients. Postoperative pathology confirmed the diagnosis of renal cancer. After the surgery, the bladder cancer tissues and corresponding normal tissues of the patients were immediately frozen and stored in liquid nitrogen for further processing.

Estimation and somatic mutation analysis
The ImmuneScore (ratio of immune components), StromalScore (ratio of stromal components), and ESTIMATE score (the aggregate of the two scores) for each tumor sample were computed utilizing the ESTIMATE package in R software (version 4.1.3)[21]. A higher score indicates a greater presence of corresponding components (immune, stromal, and tumor purity) within the tumor microenvironment (TME). Conduct differential analysis between high-immune and low-immune samples utilizing the limma package. Extract somatic mutation data for ccRCC from the TCGA database, retaining somatic variation information in mutation annotation format (MAF).

Correlation analysis between survival analysis and clinical pathological features
Survival analysis was conducted utilizing the Survminer and Survival packages in R software. Samples lacking survival information were excluded from the analysis. A total of 501 tumor samples were selected from 538 clear cell renal cell carcinoma (ccRCC) cases, with Kaplan–Meier method employed to generate survival curves. The log-rank test was applied to assess statistical significance, with a p-value threshold set at 0.05. The ggpubr package was loaded to perform correlation analysis between various scores and clinical pathological features, with statistical significance evaluated using the Wilcoxon rank sum test.

Functional enrichment analysis

To investigate biological functions and signaling pathways, we performed analyses using the Kyoto Encyclopedia of Genes and Genomes (KEGG) and Gene Ontology (GO). The R packages clusterProfiler, enrichplot, and ggplot2 were employed to assess KEGG and GO pathways, with a q-value or false discovery rate (FDR) threshold set at < 0.05 considered statistically significant.

scRNA-seq analysis

Single-cell data were analyzed using the Seurat package. The DropletUtils package was employed to differentiate between genuine cells and empty droplets. The data were preprocessed to retain cells expressing at least 200 genes, 1000 unique molecular identifiers (UMIs), and less than 20% mitochondrial gene content. The scDblFinder software package was utilized to eliminate doublets. Data normalization was performed using the ScTransform software package, followed by dimensionality reduction to 2000 variable genes through principal component analysis (PCA). The Harmony software package was used to integrate six samples into the dataset, which were subsequently clustered at a resolution of 1.0. Cell clusters were annotated based on literature searches for cell marker genes[22]. Clusters were visualized using UMAP (Uniform Manifold Approximation and Projection) or t-SNE (t-Distributed Stochastic Neighbor Embedding) dimensionality reduction techniques. The FindMarkers package was employed to identify differentially expressed genes (DEGs) between tumor samples and normal samples, utilizing the Wilcoxon rank sum test with a log2 fold change threshold of 0.5; an adjusted p-value of < 0.05 indicated statistical significance.

Cell lines and cell culture

The THP-1, 786-O and 769-P cell lines were obtained from the American Type Culture Collection (ATCC) and are maintained under specific conditions. The culture medium consisted of 0.2 mg/mL G-418, 10% fetal bovine serum (FBS), and 100 U/mL penicillin, supplemented with 100 μg/mL streptomycin (Gibco, NY, USA), and incubated at 37 °C in a humidified atmosphere containing 5% CO_2.

Generation and differentiation of macrophages

To induce differentiation into M2 macrophages, THP-1 cells were first exposed to 100 ng/mL phorbol 12-myristate 13-acetate (PMA) (MedChemExpress, USA) for a period of 24 h. Following this, the cells were further stimulated with a combination of 10 ng/mL interleukin-13 (IL-13) and 10 ng/mL interleukin-4 (IL-4) (both from MedChemExpress, USA) for an additional 48 h.

Cell transfection

The overexpression virus targeting APOC1 was provided by GIBCO. Transfection into cells was carried out in accordance with the manufacturer's instructions.

Immunohistochemistry

Tissue sections were subjected to dewaxing and dehydration, followed by antigen retrieval and inactivation. Endogenous peroxidase activity was inhibited using a 3% hydrogen peroxide solution. The sections were incubated with primary antibody at 4 °C for more than 24 h, after which they were washed and subsequently incubated with a chromogen-labeled secondary antibody. Hematoxylin was employed as a counterstain for the sections.

Immunofluorescence

Cells were seeded onto pre-treated coverslips and cultured until they reached an appropriate density. The cells were then fixed with 4% paraformaldehyde for 15 min at room temperature to preserve cellular structure. Cell membranes were permeabilized using a solution of 0.1% Triton X-100 in PBS for 10 min, allowing antibodies to access intracellular antigens. Non-specific binding sites were blocked by incubating the samples with 5% normal goat serum or bovine serum albumin (BSA) in PBS for 1 h at room temperature to reduce background signals. Specific primary antibodies were added and incubated overnight at 4 °C to ensure thorough binding to target antigens. The samples were washed three times with PBS, each wash lasting 5 min. Fluorescently labeled secondary antibodies were added and incubated for 1 h at room temperature in the dark. Unbound secondary antibodies were removed by washing the samples three times with PBS, each wash lasting 5 min. Coverslips were mounted onto glass slides using a mounting medium containing an anti-fade agent to prevent photobleaching. Samples were observed under a fluorescence microscope, and fluorescence signals were recorded and analyzed.

RNA extraction and real-time quantitative PCR

Total RNA was extracted using the Trizol method, and its purity and concentration were evaluated with a nucleic acid quantifier. Following the operating instructions of Invitrogen's 'M-MLV First-Strand Synthesis System for qRT-PCR,' 1–3 μg of total RNA was employed to establish a 20 μL reverse transcription system for cDNA synthesis. Subsequently, fluorescence amplification was performed utilizing the 'Platinum SYBR Green qPCR SuperMix-UDG with ROX' kit in conjunction with an ABI 7500 Fast Real-Time PCR system from Invitrogen.

GAPDH:
Forward Primer TCTGACTTCAAGCGACAC.
Reverse Primer CAAATTCGTTGTCATACCAG.
CD206:
Forward Primer GGGTTGCTATCACTCTCTATGC.
Reverse Primer TTTCTTGTCTGTTGCCGTAGTT.
CD163:

Forward Primer TTTGTCAACTTGAGTCCCTTCAC.
Reverse Primer TCCCGCTACACTTGTTTTCAC.
IL10:
Forward Primer GACTTTAAGGGTTACCTGGGTTG.
Reverse Primer TCACATGCGCCTTGATGTG-3′;
ARG1:
Forward Primer GTGGAAACTTGCATGGACAAC.
Reverse Primer AATCCTGGCACATCGGGAATC.
ABCA1
Forward PrimerACCCACCCTATGAACAACATGA.
Reverse PrimerGAGTCGGGTAACGGAAACAGG.
CD36
Forward PrimerCTTTGGCTTAATGAGACTGGGAC.
Reverse PrimerGCAACAAACATCACCACACCA.
Scarb1
Forward PrimerACTTCTGGCATTCCGATCAGT.
Reverse PrimerACGAAGCGATAGGTGGGGAT.
ABCG1
Forward Primer ATTCAGGGACCTTTCCTATTCGG.
Reverse Primer CTCACCACTATTGAACTTCCCG.
APOC1
Forward Primer CGGTCCTGGTGGTGGTTCTG.
Reverse Primer GTTTGATGCGGCTGATGAGTTCC.

Flow cytometry

To prepare macrophages for flow cytometry, the cells were harvested and washed twice with phosphate-buffered saline (PBS) to create single-cell suspensions. The cells were then incubated with PE-conjugated mouse anti-human CD163 antibodies (source: CN) for 30 min at 4 °C. Following incubation, the stained cells were washed twice and resuspended in 200 µL of flow buffer.Flow cytometry was performed using a FACSCalibur flow cytometer (BD Biosciences, USA), and the data were analyzed with FlowJo software.

Western blot

Cells were harvested and lysed using RIPA buffer for whole cell lysis. Total proteins were subsequently extracted, quantified, separated by 8–12% SDS-PAGE, and semi-dry transferred to PVDF membranes (Millipore, Billerica, MA, USA). The PVDF membranes were initially blocked with TBS + Tween (TBST) solution containing 5% skim milk powder for 2 h, washed, and then incubated with primary antibodies overnight at 4 °C (APOC1; catalog number: 13507–1-AP Proteintech; dilution: 1:1000). Following this incubation, the membranes were re-washed and incubated with horseradish peroxidase-conjugated secondary antibodies for 2 h. Finally, antibody binding was detected using a chemiluminescence method. A gel imaging system was employed to capture the image and quantify the gray values.

Transwell experiment

Cells were harvested using serum-free culture medium, and a concentration of 2×10^5 cells/mL was added to the upper chamber of an 8.0 µm aperture polycarbonate membrane filter (Corning, New York, USA), with or without basement membrane matrix gel (catalog number: 2251002, Corning, New York, USA) for invasion and migration assays respectively. Subsequently, 600 µL of 10% fetal bovine serum culture medium was added to the lower chamber. The cells were incubated at 37 °C for 4–6 h and then stained with a solution of 0.1% crystal violet. Each experiment included three replicate wells and was repeated three times. Random fields were selected for counting while simultaneously capturing images.

Wound-healing assay

Cells were cultured in a six-well plate until 85–90% confluence was achieved. Subsequently, a 200 µL pipette tip was utilized to create scratches on the cell monolayer. The scratches were rinsed three times prior to imaging, and the medium was replaced with 1% FBS culture medium. Following this, cells were washed three times with PBS, serum-free medium was added, and the cells were further incubated while images were captured using a microscope.

Triglyceride determination

To quantitatively measure intracellular triglyceride levels, we utilized a triglyceride assay kit (ab65336, Abcam, Cambridge, UK) following the manufacturer's instructions.

Statistical analysis

Data were analyzed using SPSS version 22.0, GraphPad Prism version 8.0, and other statistical software. Statistical tests, including t-tests and chi-square tests, were employed for data analysis. Results are expressed as mean ± SD unless otherwise specified. All experiments were conducted in triplicate or more. For all statistical analyses, p-values less than 0.05 were considered statistically significant.

Result
Analytical workflow of the study

This study was conducted following the analytical workflow outlined in Fig. 1. We began by downloading TCGA-KIRC RNA-seq data, which included 538 primary tumor samples and 72 normal tissue samples, along with corresponding clinical information from the UCSC database. The ESTIMATE algorithm was then employed to calculate the proportions of tumor-infiltrating immune cells (TICs) as well as immune and stromal components within the tumor samples. Concurrently, somatic mutation data were downloaded to assess the tumor mutation landscape between high-immune and low-immune cohorts based on median ImmuneScore values. we identified immune-related genes (IMMU genes) using median ImmuneScore thresholds and performed Gene Ontology (GO) enrichment analysis on these genes. Additionally, single-cell RNA sequencing data were integrated to determine the immune-related genes that affect the prognosis of ccRCC. Eventually, a total of 42 immune-related genes (IMDGs) were identified. To identify highly expressed immune-related genes in renal cancer, we conducted an intersection analysis between IMDGs and those differentially expressed in the renal cancer datasets GSE105261 and GSE168845. This systematic approach revealed APOC1 as a key candidate gene.

Correlation analysis of immune characteristics and prognostic features in ccRCC patients

Tumor tissue comprises not only tumor cells but also various other cell types associated with the tumor microenvironment, including normal stromal cells, immune cells, vascular endothelium, and blood cells within blood vessels[5,23]. The ESTIMATE algorithm quantifies the proportion or abundance of immune cells, stromal cells, and tumor cells relevant to the tumor microenvironment in tumor tissue [24]. The resulting ImmuneScore, StromalScore, and ESTIMATEScore were correlated with overall survival (OS), utilizing Kaplan–Meier survival analysis to elucidate the relationship between immune and stromal ratios and ccRCC patient survival. The results indicated that ImmuneScore, StromalScore, and ESTIMATEScore were positively correlated with OS ($p = 0.019$; $p = 0.023$; $p = 0.0022$) (Fig. 2A). Subsequently, clinical information from ccRCC cases was analyzed to assess correlations between these three scores and TNM classification (Fig. 2B–D), revealing that both ImmuneScore and ESTIMATEScore significantly decreased with advancing TNM classification; however, no significant correlation was observed for StromalScore. These findings underscore the critical role of immune components in ccRCC progression, particularly concerning invasion and metastasis."

Comparative analysis of somatic mutations in high- and low-immunity groups

To elucidate the landscape of tumor immune gene mutations in ccRCC, we undertook further investigations. Utilizing the median ImmuneScore, somatic mutation data from these two groups were analyzed and visualized to evaluate potential genetic differences between high-immune and low-immune populations. The results revealed the top 30 most frequently mutated genes within these cohorts (Fig. 3A–B). In comparison to the low-immune group, the high-immune group demonstrated a higher proportion of mutated genes, indicating that patients with more extensive gene mutations often exhibit increased immune infiltration.
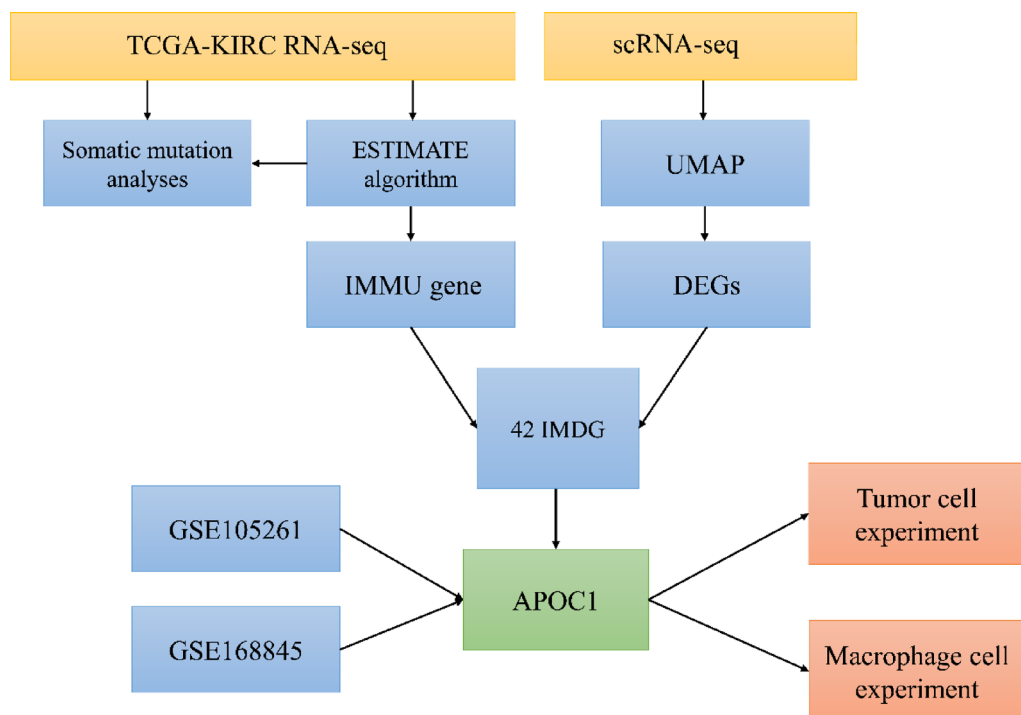
Fig. 1. Analytical Workflow of the Study.
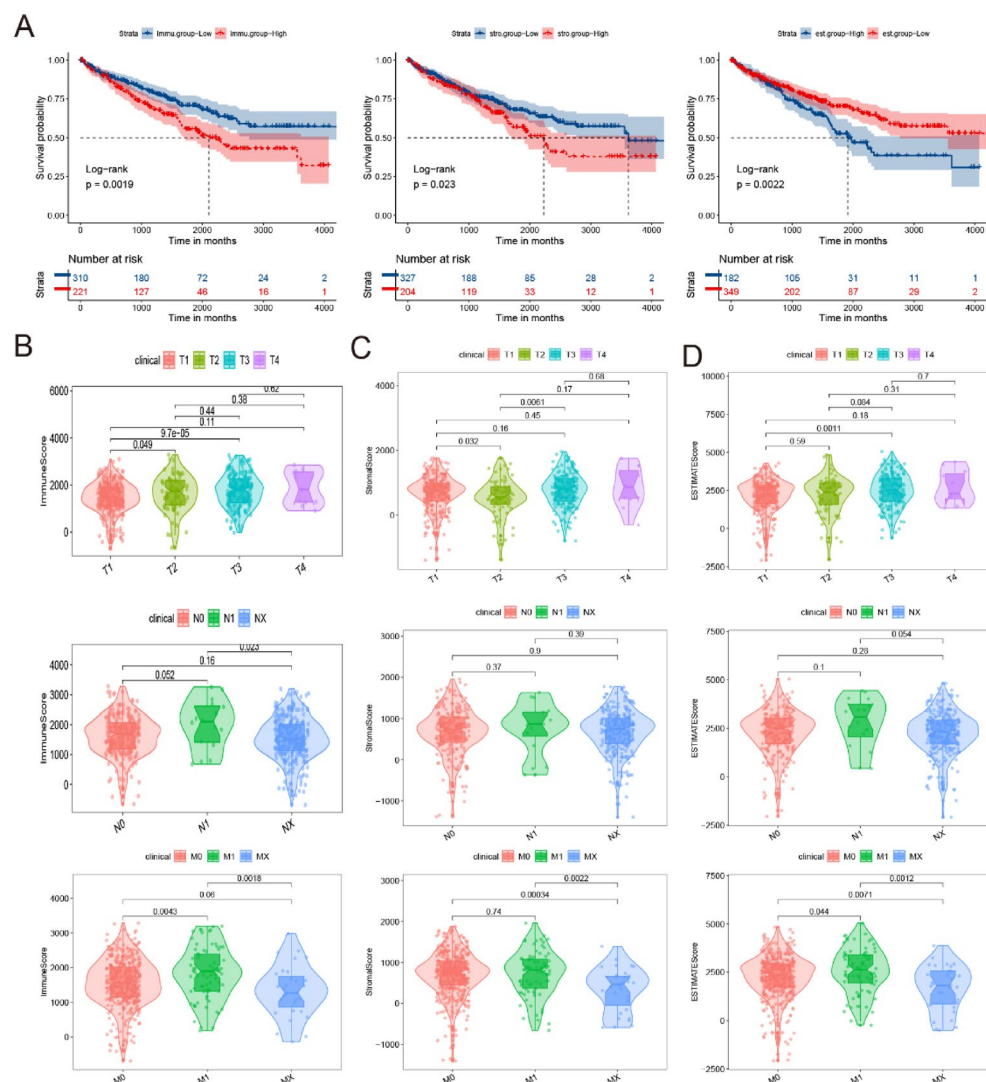
Fig. 2. Correlation analysis between immune characteristics and prognostic features of ccRCC patients. (**A**) Kaplan–Meier survival analysis for ccRCC patients grouped into high or low scores in ImmuneScore, StromalScore and ESTIMATEScore. $p = 0.0019$, 0.023 and 0.0022, (**B**–**D**) Distribution of ImmuneScore, StromalScore, and ESTIMATEScore in the T, N, M classification. respectively, by Kruskal–Wallis rank sum test.

The IMMU genes were identified based on the ImmuneScore

Investigating the factors influencing tumor immunity may offer a strategy to improve the prognosis of patients with ccRCC. Accordingly, TCGA data were stratified into high-immune and low-immune samples based on the median ImmuneScore. A volcano plot was generated to illustrate the results of differential gene analysis (P. Value < 0.05, |LogFC| > 0.5). Subsequently, the top 20 upregulated and downregulated genes were identified using the absolute value of log2 fold change (FC), and a heatmap was constructed (Fig. 4A–B). A total of 249 immune-related genes (IMMU genes) were obtained (adj.P.Val < 0.05, |LogFC| > 1). Following this, Gene Ontology (GO) analysis indicated that IMMU genes were primarily associated with immune functions such as humoral immune response mediated by circulating immunoglobulin, humoral immune response itself, immunoglobulin complex formation, and immunoglobulin receptor binding (Fig. 4C–E). Ultimately, IMMU genes were recognized as the principal gene set related to immune infiltration in ccRCC.

Single-cell analysis identifies differentially expressed genes (DEGs) between healthy controls and ccRCC samples

The advancement of single-cell RNA sequencing (scRNA-seq) has facilitated a comprehensive analysis of tumors and their microenvironments[25]. By measuring the transcriptome at the single-cell level, scRNA-seq can more accurately delineate cellular heterogeneity within tumors compared to traditional methodologies[26].

The single-cell transcriptome dataset GSE121636 was retrieved from the GEO database, and a comprehensive immune profile was generated using single-cell RNA-seq data derived from 25,000 immune cells isolated from three renal cell carcinoma tumors and their matched peripheral blood samples. Following stringent quality control measures, a total of 24,306 high-quality cells were acquired. Ultimately, 18 distinct cell clusters were
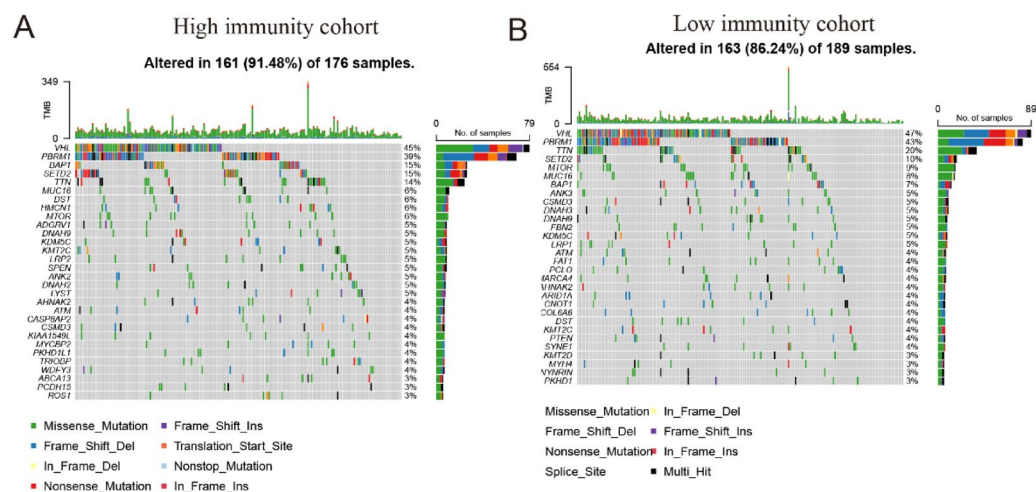
Fig. 3. Somatic mutation analyses between high- and low-immunity groups. (**A–B**) Waterfall plot shows the mutation distribution of the top 30 most frequently mutated genes. The central panel shows the types of mutations in each ccRCC sample. The upper panel shows the mutation frequency of each ccRCC sample. The bar plots on the right side show the frequency and mutation type of genes mutated in the high- and low-immunity cohort, respectively. The bottom panel is the legend for mutation types.
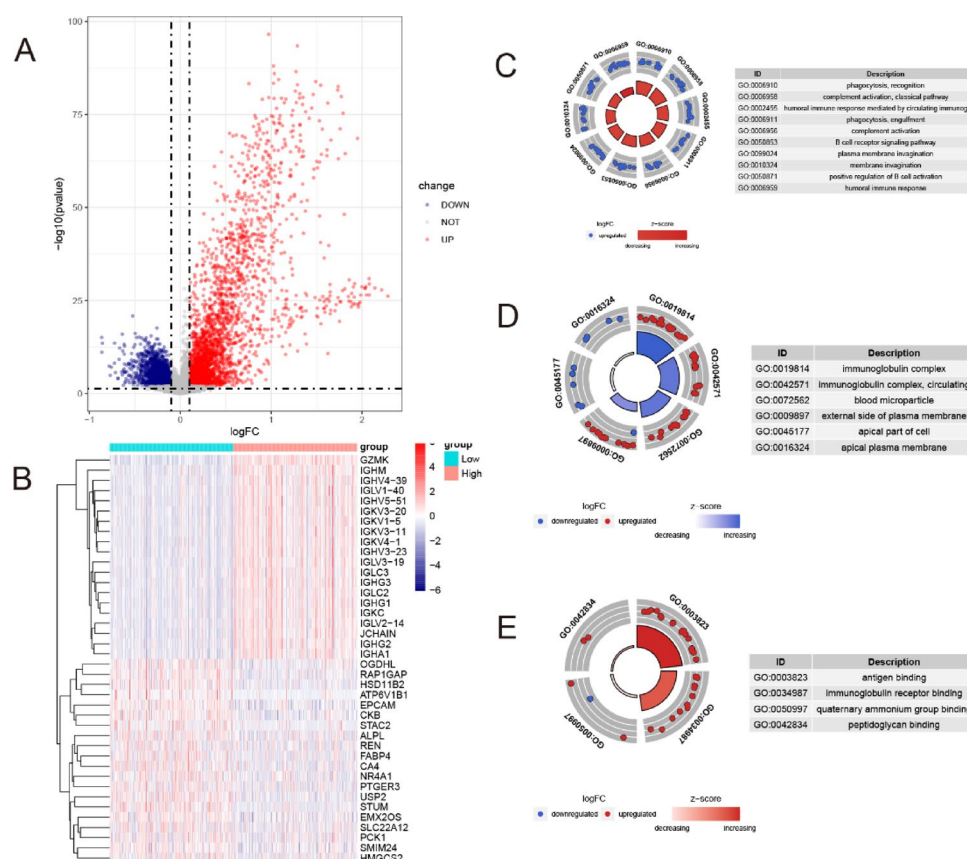

Fig. 4. The IMMU gene were identified by ImmuneScore. (**A–B**) IMMU gene generated by comparison of the high score group vs. the low score group in ImmuneScore. Volcano plot for IMMU gene (A). The blue and red dots represented the significantly downregulated and upregulated genes; and the gray dots represented the genes without differential expression. Heatmap for The IMMU gene (B). | log2 FC |> 1 and $p < 0.05$. (C-E) GO enrichment analysis for IMMU gene, terms with FDR < 0.05 were believed to be enriched significantly.

identified and classified into 10 major cell subsets, including monocytes, Macro1, Macro2, Macro3, B cells, NK cells, CD4 + T cell, CD8 + T cell, regulatory T cell and DC cells. All cell types were visualized using Uniform Manifold Approximation and Projection (UMAP) projection (Fig. 5A–B). Cell identities were manually assigned based on established marker genes in the literature (Fig. 5C).

Consequently, single-cell differential analysis was employed to identify specific differentially expressed genes (DEGs) across 10 cell types between the healthy control group and ccRCC samples. Among these, a total of 646 DEGs were identified (P.Value < 0.05, |LogFC| > 3) (Fig. 5D). Additionally, to identify immune-related genes that influence tumor progression, cross-analysis was conducted to determine overlapping genes between DEGs and IMMU genes. The results revealed the identification of 42 tumor immune-related genes (IMDGs) (Fig. 5E, Supplementary table 1). Therefore, these 42 IMDGs are regarded as immune genes that impact the progression and prognosis of ccRCC.

APOC1 is significantly upregulated in ccRCC and influences cancer progression and prognosis

We conducted differential expression analysis on the renal cancer datasets GSE105261 and GSE168845. The volcano plot revealed a set of genes with significant differential expression under varying conditions (Fig. 6A–B). To identify highly expressed immune-related genes in renal cancer, we intersected IMDGs with those differentially expressed in renal cancer, ultimately identifying APOC1 and C1QA (Fig. 6C, Supplementary table 2).
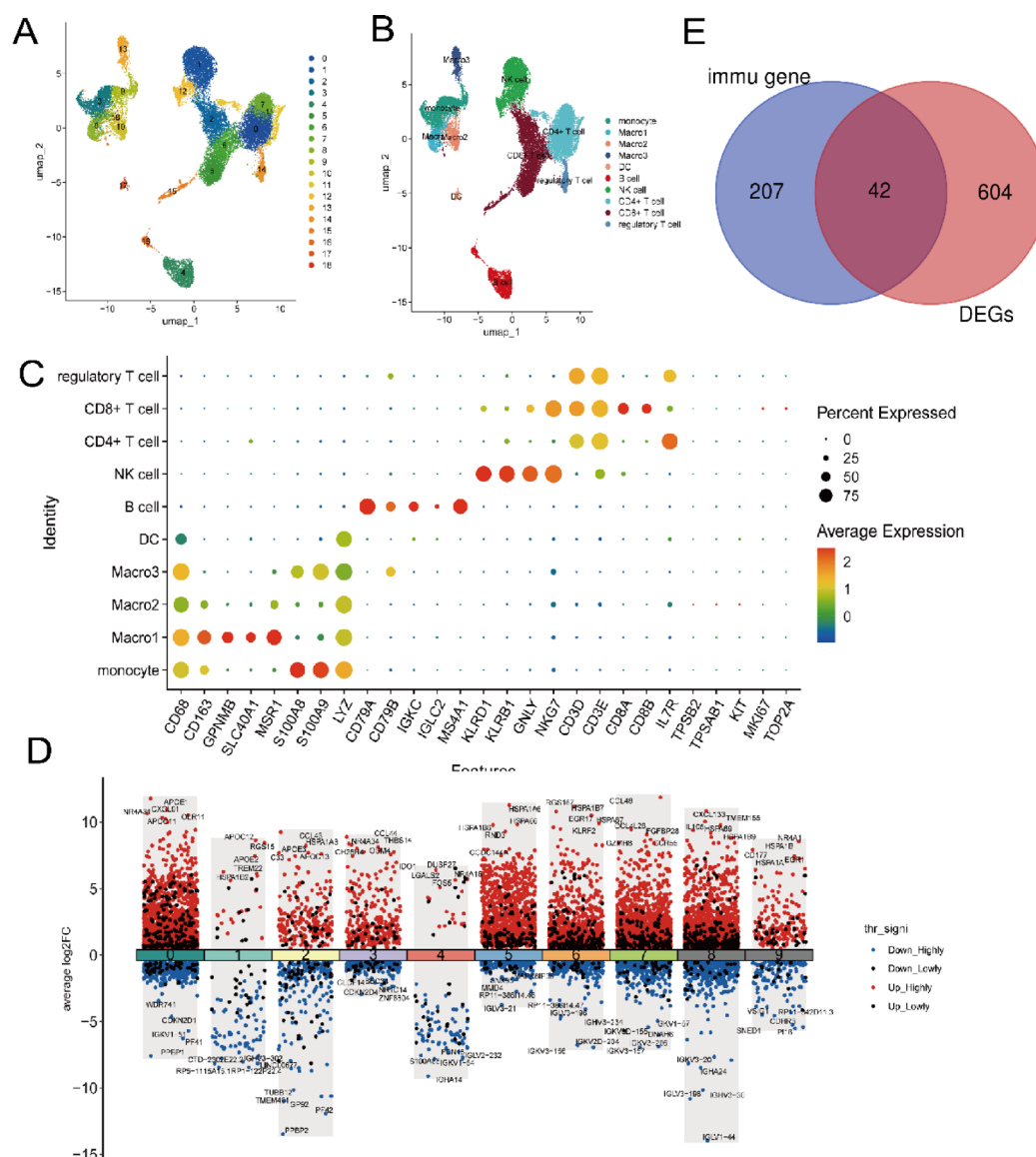
Fig. 5. Identification of DEGs between Healthy Controls and ccRCC Samples. (**A–B**) All cells were classified into ten types and displayed in the UMAP plot. (**C**) The bubble heatmap displays the marker genes of the ten cell types, with dot sizes indicating the proportion of expressed cells, colored according to expression levels. (**D**) Specific DEGs was identified in healthy control groups and cancer samples. (E) Venn diagram of IMMU gene and DEGs.
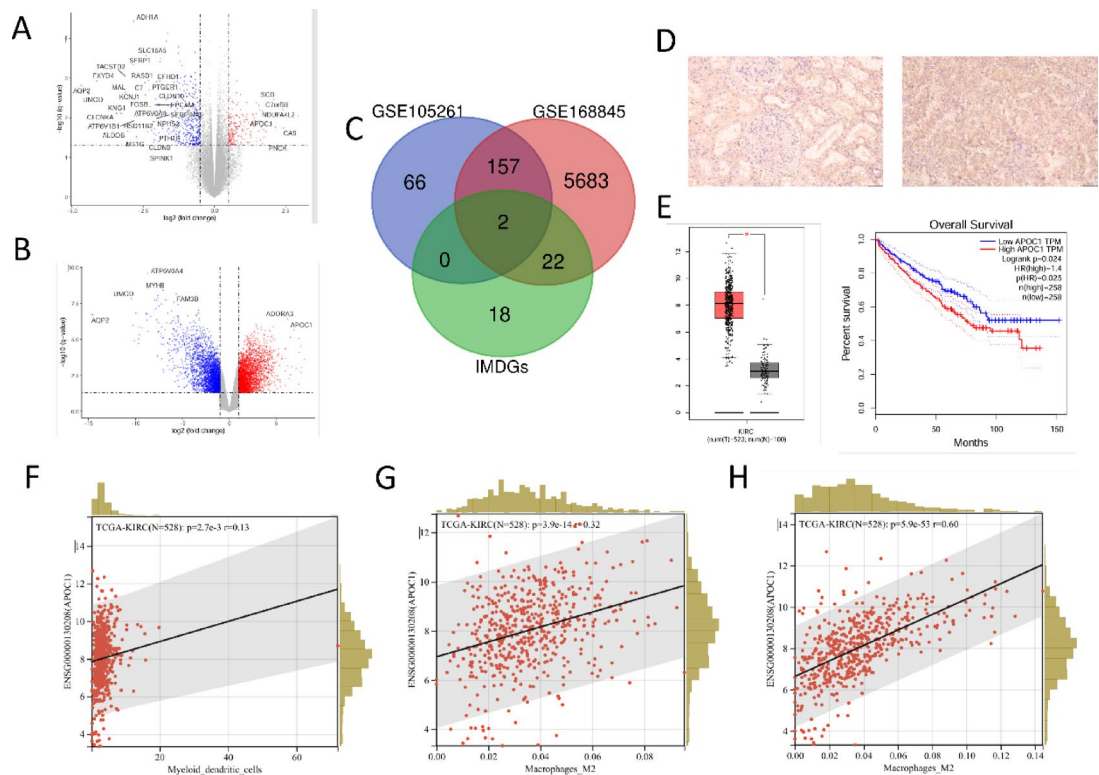
Fig. 6. APOC1 is highly expressed in renal cancer and affects macrophage immune infiltration. (**A–B**). The volcano plot illustrates the differential gene expression changes in the GSE105261 and GSE168845 datasets. Red and blue points denote significantly upregulated and downregulated genes, respectively. (**C**). The Venn diagram delineates the overlap and uniqueness of genes among the GSE105261, GSE168845 datasets, and IMDGs. (**D**). Immunohistochemical staining demonstrates elevated APOC1 expression in clear cell renal cell carcinoma (ccRCC) (Magnification: 10×20). (**E**) The box plot compares APOC1 expression levels between ccRCC samples and control groups (left panel), while the Kaplan–Meier curve assesses the impact of APOC1 expression on patient survival (right panel). (**F–H**). Scatter plots depict the correlation between APOC1 expression and macrophage infiltration as quantified by MCPcounter, QUANTISEQ, and XCELL algorithms, with regression lines and correlation coefficients provided.

Immunohistochemical analysis of 10 paired samples of renal cancer and adjacent non-tumor tissues demonstrated that APOC1 was significantly upregulated in cancerous tissues (Fig. 6D), while no significant difference was observed for C1QA (Fig. S1). Data from the GEPIA database confirmed that APOC1 is overexpressed in renal cancer and is associated with poor prognosis (Fig. 6E). Furthermore, a scatter plot analysis revealed a significant positive correlation between APOC1 expression levels and macrophage infiltration, suggesting that APOC1 may play a role in macrophage-mediated immune regulation in renal cancer (Fig. 6F–H).

Overexpression of APOC1 promoted the migration and invasion of clear cell renal cell carcinoma (ccRCC) cells in vitro

To investigate the effects of APOC1 overexpression on ccRCC, we conducted a series of in vitro experiments. Initially, we overexpressed APOC1 in two ccRCC cell lines. PCR confirmed that APOC1 expression levels in the oeAPOC1 group were significantly higher compared to the control group (Fig. 7A–B). The Transwell invasion assay revealed that the number of migrating cells in the oeAPOC1 group was markedly increased relative to the control group, indicating enhanced invasive capability (Fig. 7C). Additionally, scratch assays demonstrated that after 24 h, the wound closure area in the oeAPOC1 group was significantly smaller than that in the control group for both 786-O and 769-P cells (Fig. 7D). These findings suggest that APOC1 overexpression promotes ccRCC cell migration and invasion in vitro.

APOC1 exhibits high expression levels in macrophages and influences their polarization toward the M2 phenotype

In this study, human THP-1 monocytes were first differentiated into M0 macrophages by treating them with PMA for 24 h. Subsequently, these M0 macrophages were further differentiated into M2-type tumor-associated macrophages by exposing them to IL-4 and IL-13 for an additional 48 h in the continued presence of PMA (Figure S2A). RT-qPCR analysis revealed that compared to THP-1 monocytes, M0 macrophages showed increased expression of the CD11b gene. Moreover, M2 macrophages exhibited significantly higher expression levels of M2 marker genes such as CD163, CD206, IL10, and ARG1, while the expression of M1 marker genes like iNOS and
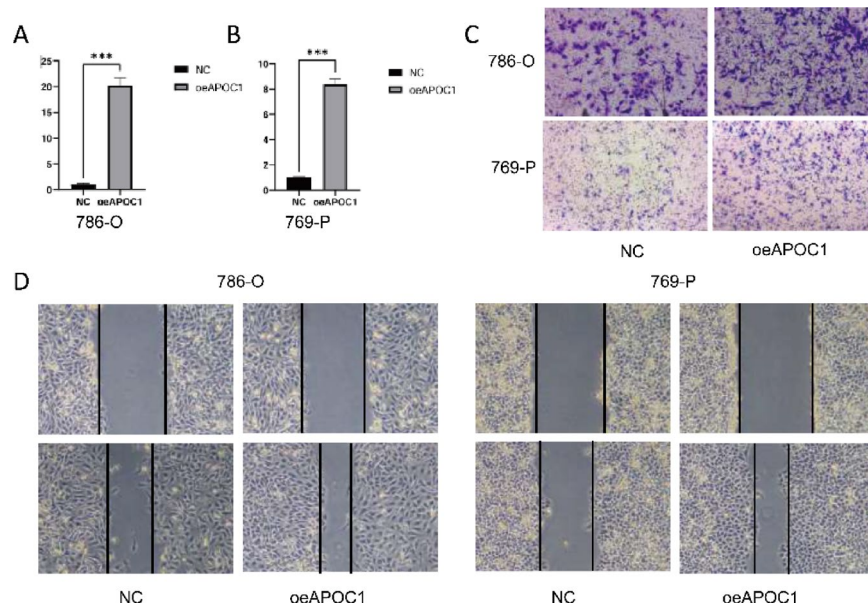
Fig. 7. APOC1 overexpression significantly enhanced the migratory and invasive capabilities of ccRCC cells. (**A–B**) The PCR test results indicated that in the 786-O and 769-P cell lines, the APOC1 overexpression group and the control group had different gene expressions. (**C**) 786-O (up) and 769-P (down) cell migration assay. (**D**) 786-O (left) and 769-P (right) cell Wound-Healing Assay. ns, $p \geq 0.05$; ***$p < 0.05$; ****$p < 0.01$.
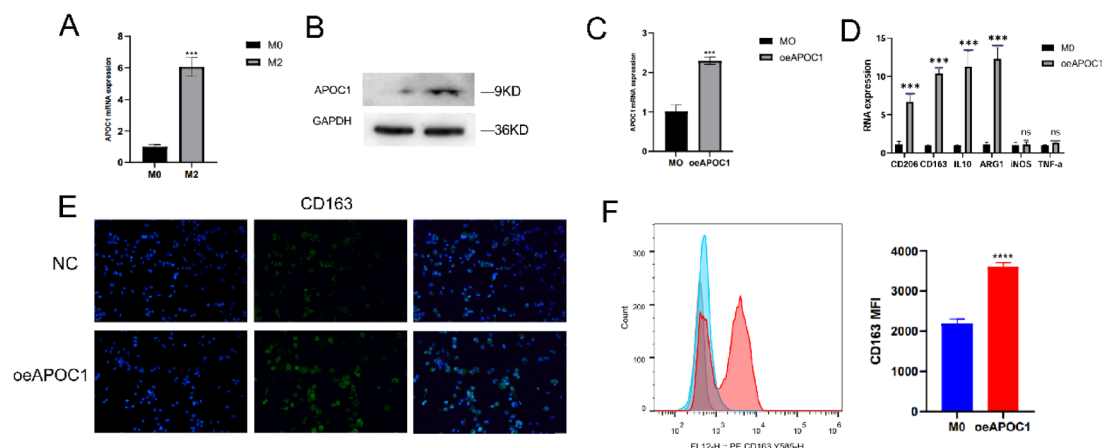
Fig. 8. APOC1 polarizes macrophages into M2-type TAMs. (A-B) The expression of APOC1 in M2 macrophages was determined by RT-PCR (**A**) and Western blotting (**B**). (**C**) The expression of APOC1 in APOC1-overexpressing macrophages and non-overexpressing macrophages was determined by RT-PCR. (**D**) The expression of M2 macrophage markers (CD163, CD206, ARG1 and IL10) and M1 macrophage markers (TNF-α and iNOS) in M2 macrophages was determined by PCR. (**E–F**) The expression of M2 macrophage marker CD163 was verified by immunofluorescence and flow cytometry. ns, $p \geq 0.05$; ***$p < 0.05$; ****$p < 0.01$.

TNF-α remained unchanged (Fig. S2B–C). Flow cytometry results corroborated these findings, demonstrating a substantial increase in the protein levels of M2 markers (CD163 and CD206) in M2 macrophages compared to M0 macrophages (Fig. S2D–E). These findings collectively suggest that THP-1 monocytes can be successfully transformed into M2-type tumor-associated macrophages.

To investigate the role of APOC1 in facilitating the polarization of macrophages toward M2-type TAMs, we performed RT-qPCR and Western blot analyses. Our findings revealed a significant upregulation of APOC1 expression in M2 macrophages relative to M0 macrophages (Fig. 8A–B). We then proceeded to overexpress the APOC1 gene in macrophages (Fig. 8C). RT-qPCR data confirmed that the expression levels of M2-type macrophage marker genes, including CD163, CD206, IL10, and ARG1, were substantially elevated in macrophages with APOC1 overexpression, whereas the expression of M1-type macrophage markers, such as iNOS and TNF-α, remained unaffected (Fig. 8D). Immunofluorescence and flow cytometry analyses further corroborated these observations, demonstrating that APOC1 overexpression enhances the polarization of
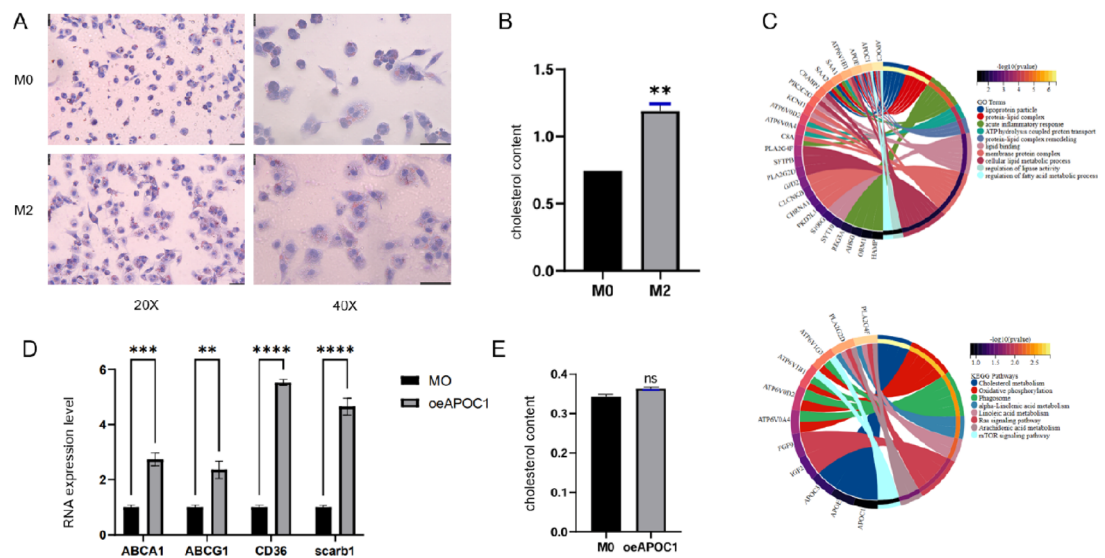
Fig. 9. APOC1 affects cholesterol transport in macrophages. (**A**) The Oil Red experiment shows the lipid content of M0 and M2 macrophages. (**B**) Cholesterol determination shows the cholesterol content of M0 and M2 macrophages. (**C**) GO and KEGG analysis diagrams. (**D**) RT-PCR demonstrates the expression levels of cholesterol uptake genes (CD36 and scarb1) and cholesterol efflux genes (ABCA1 and ABCG1). (**E**) Cholesterol determination shows the changes in cholesterol after overexpression of APOC1. ns, $p \geq 0.05$; ***$p < 0.05$; ****$p < 0.01$.

macrophages toward an M2 phenotype (Fig. 8E–F). Collectively, these results underscore the critical role of APOC1 in promoting the polarization of M2-type TAMs in ccRCC.

APOC1 influences cholesterol transport in macrophages

Lipid synthesis plays a pivotal role in the polarization of macrophages, particularly during M2 polarization, which requires reprogramming of lipid synthesis pathways to support its anti-inflammatory and tissue repair functions[27]. Dynamic changes in lipid metabolism can direct the polarization of macrophages. Alterations in the activities of fatty acid synthase (FAS), acetyl-CoA carboxylase (ACC), and cholesterol metabolic pathways modulate the functional state of macrophages. Oil Red O staining revealed that M2 macrophages exhibit higher lipid content compared to M0 macrophages (Fig. 9A). Cholesterol quantification experiments demonstrated a significant increase in cholesterol levels in M2 macrophages (Fig. 9B). Gene Ontology (GO) and KEGG pathway analyses indicated that APOC1 is involved in cholesterol transport pathways (Fig. 9C)[28,29]. Overexpression of APOC1 resulted in a marked upregulation of genes associated with cholesterol uptake (CD36 and SCARB1) and efflux (ABCA1 and ABCG1) in macrophages (Fig. 9D). However, overexpression of APOC1 did not alter the overall cholesterol content within macrophages (Fig. 9E). These findings suggest that APOC1 primarily regulates cholesterol transport rather than intracellular cholesterol metabolism in macrophages.

Discussion

Renal cell carcinoma (RCC) accounts for over 90% of malignant renal tumors, with clear cell renal cell carcinoma (ccRCC) representing the most prevalent subtype[30,31]. A range of immunotherapeutic approaches, including anti-PD-1, anti-PD-L1, and anti-CTLA-4 antibodies, in conjunction with various targeted therapies, have shown substantial progress in managing metastatic ccRCC[32]. Nevertheless, the clinical utility of these agents is significantly constrained by their efficacy and associated adverse effects[33]. Therefore, there is an urgent imperative to elucidate tumor pathogenesis and identify novel therapeutic targets. In recent years, the tumor microenvironment (TME) has attracted increasing scholarly attention as a focal point of research due to its complex composition and dynamic nature that are pivotal in tumorigenesis and cancer progression[34,35]. Exploring new mechanisms through which both tumors and their microenvironments modulate cancer progression may unveil promising immune targets for enhancing diagnostic and therapeutic strategies for ccRCC.

In recent years, single-cell RNA sequencing (scRNA-seq) technology has advanced rapidly and has been widely adopted in various fields[36]. scRNA-seq offers higher sensitivity and enhanced cell processing capabilities, enabling a comprehensive elucidation of transcriptome characteristics. We obtained transcriptome RNA-seq data from the Cancer Genome Atlas (TCGA) database and integrated this with the ESTIMATE algorithm and single-cell data to analyze immune-related prognostic markers within TME. This approach led to the identification of 42 IMDGs. By cross-analyzing these IMDGs with differentially expressed genes in the ccRCC dataset, we confirmed that APOC1 is highly expressed in ccRCC and influences the migration and proliferation of ccRCC cells. TAMs, which constitute approximately 50% of hematopoietic cells in the TME, play a critical role in tumor development. Subsequent immune infiltration analysis revealed a strong correlation between APOC1

expression and macrophage infiltration. Further experiments demonstrated that APOC1 is highly expressed in macrophages and plays a significant role in their polarization toward the M2 type macrophages.

APOC1 is highly expressed in renal cancer and exerts important functions in macrophages. However, the specific mechanisms by which APOC1 operates within macrophages remain unclear. Studies have shown that lipid synthesis plays a crucial role in macrophage polarization[37]. Our experimental findings indicate that the polarization of M2 macrophages is accompanied by substantial lipid accumulation and increased cholesterol synthesis. As an important member of the apolipoprotein family, APOC1 plays a key role in the metabolism of very low-density lipoprotein (VLDL) and high-density lipoprotein (HDL)[38]. Functional enrichment analysis revealed that APOC1 affects cellular cholesterol transport. Whether APOC1 influences macrophage polarization through its effects on cholesterol synthesis warrants further investigation.

This study elucidates the complex role of APOC1 in regulating macrophage functions, particularly in the polarization of M2-like TAMs and cholesterol transport. Our results suggest that although APOC1 participates in cholesterol transport in macrophages, it does not significantly affect total intracellular cholesterol content. This finding suggests that APOC1 is not involved in cholesterol accumulation but rather promotes macrophage polarization by influencing the speed of cholesterol transport within macrophages. It may increase the lipid content within macrophages by accelerating lipid metabolism or metabolic reprogramming of macrophages, thereby promoting macrophage polarization.

Furthermore, the impact of APOC1 on cholesterol transport may involve the dynamic balance of cholesterol rather than its total content. APOC1 may regulate the distribution of cholesterol among different membrane structures or organelles within the cell, rather than changing its overall amount. This regulation could affect membrane fluidity, the assembly of signaling complexes, or endoplasmic reticulum stress responses, thereby indirectly influencing macrophage function and immune responses. Further experiments are necessary to validate these hypotheses.

Nonetheless, this study presents several limitations. (1) While the study utilized data from the TCGA database, relying exclusively on public databases may result in an insufficient sample size. Expanding the sample size to include specimens from diverse racial and geographic backgrounds would enhance the reliability and generalizability of the findings. (2) Although the current experimental validation has been primarily conducted in vitro, providing valuable preliminary insights, in vivo experiments are essential to confirm the physiological role of APOC1. Utilizing mouse models or other appropriate animal models can elucidate the in vivo mechanisms of APOC1's action. (3) The relationship between APOC1 and immune infiltration is multifaceted and influenced by various factors. Therefore, incorporating additional clinical parameters and molecular markers into the analysis would provide a more comprehensive understanding of its role within the tumor microenvironment. (4) a substantial number of clinical samples are crucial for evaluating APOC1's impact on ccRCC immunity and its potential application in immunotherapy. Addressing these limitations will enable future research to more accurately delineate the biological functions of APOC1 in renal clear cell carcinoma and inform the development of personalized therapeutic.

Conclusion

APOC1 is highly expressed in ccRCC and promotes the migration and proliferation of ccRCC. Meanwhile, APOC1 promotes the polarization of macrophages towards the M2 type by enhancing cholesterol transport within macrophages. Targeting APOC1 may improve the prognosis of patients with advanced ccRCC.

Data availability

The datasets used in the current study are openly available in TCGA (https://portal.gdc.cancer.gov/) database, UCSC Xena data portal (https://xenabrowser.net/), GEO (https://www.ncbi.nlm.nih.gov/geo/) database. All date and materials are available from the corresponding authors upon request.

References
1. Hsieh, J. J. et al. Renal cell carcinoma. *Nat. Rev. Dis. Primers.* **3**, 17009. https://doi.org/10.1038/nrdp.2017.9 (2017).
2. Choueiri, T. K. & Motzer, R. J. Systemic Therapy for Metastatic Renal-Cell Carcinoma. *N. Engl. J. Med.* **376**, 354–366. https://doi.org/10.1056/NEJMra1601333 (2017).
3. Makhov, P. et al. Resistance to systemic therapies in clear cell renal cell carcinoma: Mechanisms and management strategies. *Mol. Cancer Ther.* **17**, 1355–1364. https://doi.org/10.1158/1535-7163.Mct-17-1299 (2018).
4. Atkins, M. B. & Tannir, N. M. Current and emerging therapies for first-line treatment of metastatic clear cell renal cell carcinoma. *Cancer Treat. Rev.* **70**, 127–137. https://doi.org/10.1016/j.ctrv.2018.07.009 (2018).
5. Pitt, J. M. et al. Targeting the tumor microenvironment: Removing obstruction to anticancer immune responses and immunotherapy. *Annals of oncology :Official journal of the European Society for Medical Oncology* **27**, 1482–1492. https://doi.org/10.1093/annonc/mdw168 (2016).
6. Li, Y. et al. Histopathologic and proteogenomic heterogeneity reveals features of clear cell renal cell carcinoma aggressiveness. *Cancer Cell* **41**, 139-163.e117. https://doi.org/10.1016/j.cell.2022.12.001 (2023).
7. Lee, C. H. et al. Phase II Trial of Cabozantinib Plus Nivolumab in Patients With Non-Clear-Cell Renal Cell Carcinoma and Genomic Correlates. *Journal of clinical oncology: Official journal of the American Society of Clinical Oncology* **40**, 2333–2341. https://doi.org/10.1200/jco.21.01944 (2022).
8. Iacovelli, R. et al. Current evidence for second-line treatment in metastatic renal cell carcinoma after progression to immune-based combinations. *Cancer Treat. Rev.* **105**, 102379. https://doi.org/10.1016/j.ctrv.2022.102379 (2022).
9. Christofides, A. et al. The complex role of tumor-infiltrating macrophages. *Nat. Immunol.* **23**, 1148–1156. https://doi.org/10.1038/s41590-022-01267-2 (2022).

10. Li, M. et al. Leptin decreases Th17/Treg ratio to facilitate neuroblastoma via inhibiting long-chain fatty acid catabolism in tumor cells. *Oncoimmunology* **14**, 2460281. https://doi.org/10.1080/2162402x.2025.2460281 (2025).

11. Wiecken, M. et al. The immune checkpoint LAG-3 is expressed by melanoma cells and correlates with clinical progression of the melanoma. *Oncoimmunology* **14**, 2430066. https://doi.org/10.1080/2162402x.2024.2430066 (2025).

12. Ghebremedhin, A. *et al.* Tumor-Associated Macrophages as Major Immunosuppressive Cells in the Tumor Microenvironment. *Cancers* **16**, https://doi.org/10.3390/cancers16193410 (2024).

13. Liu, J. et al. Lipid-related FABP5 activation of tumor-associated monocytes fosters immune privilege via PD-L1 expression on Treg cells in hepatocellular carcinoma. *Cancer Gene Ther.* **29**, 1951–1960. https://doi.org/10.1038/s41417-022-00510-0 (2022).

14. Sesarman, A. et al. Targeting of M2 macrophages with IL-13-functionalized liposomal prednisolone inhibits melanoma angiogenesis in vivo. *J. Liposome Res.* **34**, 535–546. https://doi.org/10.1080/08982104.2024.2315452 (2024).

15. Aydin, S., Darko, K., Detchou, D. & Barrie, U. A call for clinical trials in glioblastoma multiforme for interleukin 4, interleukin 6, interleukin 13 and CD40. *Neurosurg. Rev.* **47**, 571. https://doi.org/10.1007/s10143-024-02823-0 (2024).

16. Gao, Y. et al. Integrating single-cell RNA-seq and bulk RNA-seq to explore prognostic value and immune landscapes of methionine metabolism-related signature in breast cancer. *Front. Genet.* **15**, 1521269. https://doi.org/10.3389/fgene.2024.1521269 (2024).

17. Kulminski, A. M. et al. Association of APOE alleles and polygenic profiles comprising APOE-TOMM40-APOC1 variants with Alzheimer's disease neuroimaging markers. *Alzheimer's Dementia* https://doi.org/10.1002/alz.14445 (2024).

18. Ren, L. et al. Systematic pan-cancer analysis identifies APOC1 as an immunological biomarker which regulates macrophage polarization and promotes tumor metastasis. *Pharmacol. Res.* **183**, 106376. https://doi.org/10.1016/j.phrs.2022.106376 (2022).

19. Tang, W. et al. Upregulation of APOC1 Promotes Colorectal Cancer Progression and Serves as a Potential Therapeutic Target Based on Bioinformatics Analysis. *Journal of oncology* **2023**, 2611105. https://doi.org/10.1155/2023/2611105 (2023).

20. Yang, S., Du, J., Wang, W., Zhou, D. & Xi, X. APOC1 is a prognostic biomarker associated with M2 macrophages in ovarian cancer. *BMC Cancer* **24**, 364. https://doi.org/10.1186/s12885-024-12105-z (2024).

21. Yoshihara, K. et al. Inferring tumour purity and stromal and immune cell admixture from expression data. *Nat. Commun.* **4**, 2612. https://doi.org/10.1038/ncomms3612 (2013).

22. Massenet-Regad, L. *et al.* Large-scale analysis of cell-cell communication reveals angiogenin-dependent tumor progression in clear cell renal cell carcinoma. *iScience* **26**, 108367, https://doi.org/10.1016/j.isci.2023.108367 (2023).

23. Jarosz-Biej, M., Smolarczyk, R., Cichoń, T. & Kułach, N. Tumor Microenvironment as A "Game Changer" in Cancer Radiotherapy. *International journal of molecular sciences* **20**, https://doi.org/10.3390/ijms20133212 (2019).

24. Liao, Z. et al. A novel prognostic signature and immune microenvironment characteristics associated with disulfidptosis in papillary thyroid carcinoma based on single-cell RNA sequencing. *Frontiers in cell and developmental biology* **11**, 1308352. https://doi.org/10.3389/fcell.2023.1308352 (2023).

25. Papalexi, E. & Satija, R. Single-cell RNA sequencing to explore immune cell heterogeneity. *Nat. Rev. Immunol.* **18**, 35–45. https://doi.org/10.1038/nri.2017.76 (2018).

26. Chen, H., Ye, F. & Guo, G. Revolutionizing immunology with single-cell RNA sequencing. *Cell. Mol. Immunol.* **16**, 242–249. https://doi.org/10.1038/s41423-019-0214-4 (2019).

27. Yorek, M. *et al.* FABP4-mediated lipid accumulation and lipolysis in tumor-associated macrophages promote breast cancer metastasis. *eLife* **13**, https://doi.org/10.7554/eLife.101221 (2024).

28. Kanehisa, M., Furumichi, M., Sato, Y., Matsuura, Y. & Ishiguro-Watanabe, M. KEGG: Biological systems database as a model of the real world. *Nucleic Acids Res.* **53**, D672-d677. https://doi.org/10.1093/nar/gkae909 (2025).

29. Kanehisa, M. Toward understanding the origin and evolution of cellular organisms. *Protein science :A publication of the Protein Society* **28**, 1947–1951. https://doi.org/10.1002/pro.3715 (2019).

30. Tan, S. K., Hougen, H. Y., Merchan, J. R., Gonzalgo, M. L. & Welford, S. M. Fatty acid metabolism reprogramming in ccRCC: Mechanisms and potential targets. *Nat. Rev. Urol.* **20**, 48–60. https://doi.org/10.1038/s41585-022-00654-6 (2023).

31. Jonasch, E., Walker, C. L. & Rathmell, W. K. Clear cell renal cell carcinoma ontogeny and mechanisms of lethality. *Nat. Rev. Nephrol.* **17**, 245–261. https://doi.org/10.1038/s41581-020-00359-2 (2021).

32. Choueiri, T. K. & Kaelin, W. G. Jr. Targeting the HIF2-VEGF axis in renal cell carcinoma. *Nat. Med.* **26**, 1519–1530. https://doi.org/10.1038/s41591-020-1093-z (2020).

33. Wettersten, H. I., Aboud, O. A., Lara, P. N. Jr. & Weiss, R. H. Metabolic reprogramming in clear cell renal cell carcinoma. *Nat. Rev. Nephrol.* **13**, 410–419. https://doi.org/10.1038/nrneph.2017.59 (2017).

34. Peng, C. et al. TME-Related Biomimetic Strategies Against Cancer. *Int. J. Nanomed.* **19**, 109–135. https://doi.org/10.2147/ijn.S441135 (2024).

35. Yang, P. *et al.* Novel targets for gastric cancer: The tumor microenvironment (TME), N6-methyladenosine (m6A), pyroptosis, autophagy, ferroptosis and cuproptosis. *Biomedicine & pharmacotherapy = Biomedecine & pharmacotherapie* **163**, 114883, https://doi.org/10.1016/j.biopha.2023.114883 (2023).

36. Huang, G., Yu, Y., Su, H., Gan, H. & Chu, L. Integrating RNA-seq and scRNA-seq to explore the prognostic features and immune landscape of exosome-related genes in breast cancer metastasis. *Ann. Med.* **57**, 2447917. https://doi.org/10.1080/07853890.2024.2447917 (2025).

37. Bonilla, M. E. *et al.* Metabolic landscape of the healthy pancreas and pancreatic tumor microenvironment. *JCI insight* **9**, https://doi.org/10.1172/jci.insight.180114 (2024).

38. Chen, H. et al. Multifunctional porphyrinic metal-organic framework-based nanoplatform regulating reactive oxygen species achieves efficient imaging-guided cascaded nanocatalytic therapy. *J. Colloid Interface Sci.* **684**, 423–438. https://doi.org/10.1016/j.jcis.2025.01.041 (2025).

Acknowledgements

Author contributions

GF: Conceptualization, Formal analysis, Funding acquisition, Writing – review & editing; WH: Data curation, Formal analysis, Methodology; MZ: Data curation; Formal analysis, Resources, Visualization; HZ: Conceptualization, Project administration, Supervision, Writing-review & editing, Funding acquisition. All authors have read and approved the final manuscript.

Funding

Declarations

Competing interests
The authors declared no potential conflicts of interest with respect to the research, authorship, and/or publication of this article.

Ethics approval and consent to participate
The clinical specimens used in this study were all collected from patients with their explicit consent. The ethical approval was approved by the Second Hospital of Hebei Medical University.

Consent for publications
Not applicable.

Additional information
Supplementary Information The online version contains supplementary material available at https://doi.org/10.1038/s41598-025-18392-1.

Correspondence and requests for materials should be addressed to Z.H.

Reprints and permissions information is available at www.nature.com/reprints.

Publisher's note Springer Nature remains neutral with regard to jurisdictional claims in published maps and institutional affiliations.